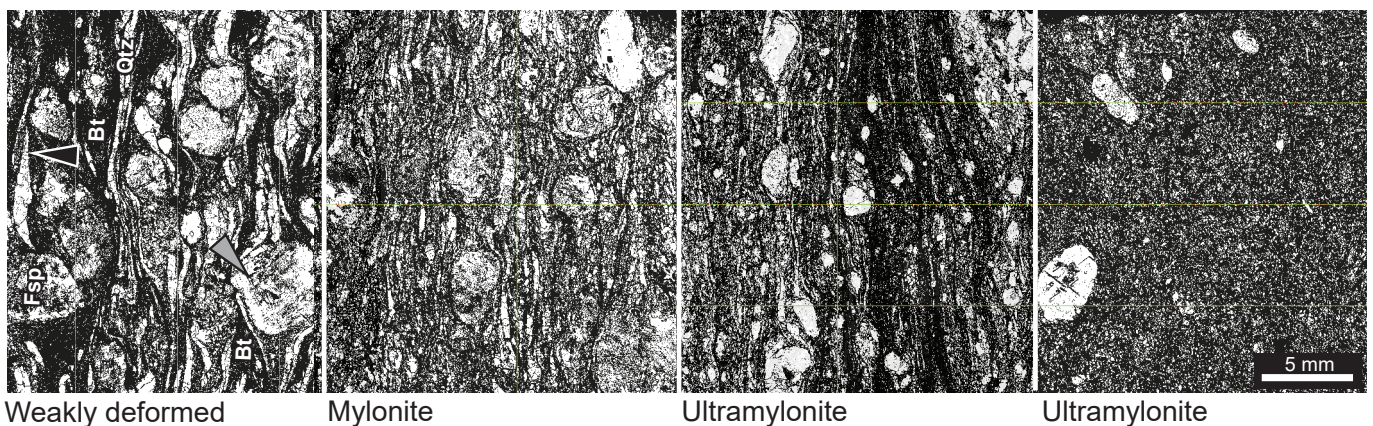


## SUPPLEMENTARY INFORMATION

## Sample location and description

Nearly all samples used in this study come from a 1 km-thick band of ultramylonite in the PSZ (Fig. 1), the exceptions are samples from location SQ183 that come from a weakly-deformed lithon that grades into the ultramylonitic band. Within the ultramylonitic band, ultramylonites grade into lithons of mylonites and weakly-deformed rocks up to ~10 m thick. In these lower-strain lithons, gradational contacts between granitic diatexites, mylonites and ultramylonites suggest that the protolith to the entire ultramylonitic band was granitic diatexite, as argued in Finch et al. (2015). This interpretation is supported by geochemical similarities between weakly deformed rocks, mylonites, and ultramylonites, demonstrated in Finch et al. (2015). Consequently, we interpret that differences in deformation intensity are not a result of lithology changes. With increasing degree of mylonitisation there is a concomitant increase in the degree of phase mixing and matrix homogenisation (Fig. DR1). The five ultramylonitic samples are sourced from five different locations that are separated by lower-strain lithons and span an 850 m-thick section of the 1 km-thick ultramylonitic layer (Fig. 1). Since these are highly strained we expect that rocks across the ultramylonitic layer were initially very far apart (several km or 10s of km) and that stretching and folding of the rocks homogenised original heterogeneities (Finch et al., 2015). We argue therefore that it is unlikely that ultramylonitic rocks were a single homogenous dry protolith, different from those of the weakly-deformed lithons, and that the water contents are actually a result of shearing and water loss.



**Fig. DR1.** Characteristic microstructural changes from protomylonite to ultramylonite. Protomylonites typically exhibit an anisotropic matrix comprising large feldspar porphyroclasts (grey arrow) and dynamically recrystallised quartz ribbons (black arrow). Ultramylonites, by contrast, comprise a fine-grained equigranular matrix with lower proportions of feldspar clasts. Images captured using G50 Fabric Analyser.

While we tried to avoid using two samples from the same outcrop, the large number of retrogressed samples in ultramylonites, and the small number of weakly-deformed rocks, meant some co-located samples needed to be used to provide sufficient power ( $n$ ) for the statistical tests. However, these samples differed in appearance and were from different layers within the outcrop. Where two samples have the same number (e.g., SQ183a, SQ183b) they are from the same outcrop, up to 20m apart. One outcrop, SQ32, contained both ultramylonites and mylonites and samples of both rock types were used in this study. Weakly-deformed samples were taken from low-strain lithons within the ultramylonite layer (SQ77) and above the ultramylonitic layer (SQ183). From location SQ183 to location SQ187, weakly-deformed rocks grade into mylonites and ultramylonites and, while ultramylonites at SQ187 were too retrogressed for inclusion in this study, mylonites from the same outcrop and weakly-deformed rocks from SQ183 were not retrogressed and were included in this study.

The matrix grain size was calculated using the Feret diameter. Thin section thickness (Table DR1) was consistent over the area of the thin section and measured using a Mitutoyo digimatic micrometer with a resolution of 1  $\mu\text{m}$ . Thin sections were between ~50 and 75  $\mu\text{m}$  thick (Tables DR1 and DR2). Thin sections were scanned and photo-mosaic maps created in crossed-polarised light for grain identification.

TABLE DR1. SAMPLE DATA AND RESULTS FOR QUARTZ GRAINS

Deformation Intensity	Position	Sample	Thickness (cm)	n	Mean (H:10° Si)	Standard deviation
Weakly-deformed rocks	Matrix	sq183a	0.0051	16	3180	1727
		sq183b	0.0050	6	2795	2559
		sq77a	0.0057	8	3787	2782
		Overall		30	3265	2160
	Ribbons	sq183a	0.0051	2	7720	100
		sq183b	0.0050	14	4027	625
		sq77a	0.0057	10	4225	3126
		Overall		26	4387	2167
Mylonites	Matrix	sq30a	0.0051	9	2532	1282
		sq32a	0.0055	17	2391	1742
		sq187d	0.0049	12	2111	782
		Overall		38	2336	1370
	Ribbons	sq30a	0.0051	13	1971	831
		sq32a	0.0055	17	3270	1458
		sq187d	0.0049	11	2520	1175
		Overall		41	2657	1312
Ultramytonites	Matrix	sq29b	0.0076	14	1004	677
		sq32b	0.0069	20	1538	701
		sq32c	0.0067	18	1751	1013
		sq79a	0.0069	27	1266	439
		sq83	0.0052	6	2198	768
		Overall		85	1455	768
	Ribbons	sq29b	0.0076	1	500	0
		Overall		43	1357	626

## Method

### Crystallographic preferred orientation (CPO) of quartz

In order to investigate variations in deformation mechanism across the protomylonite, mylonite and ultramylonite suite, we measured the crystallographic preferred orientation (CPO) of the (0001) *c*-axis in quartz using a G50 Fabric Analyser at Monash University. The measured *c*-axis data was processed using the analysis software INVESTIGATOR (Wilson et al., 2007) and projected onto lower hemispheric pole figures for comparison.

### FTIR measurement

Water content was measured in individual grains in the matrix, quartz ribbons, and in feldspar porphyroclasts, where measurements were separated into those within the porphyroclast edge (within 0.25 mm of the grain boundary) and those within the core of porphyroclasts (Fig. DR2). Optically-clear regions were identified using the reflected-light microscope with the aid of photo-mosaic maps. No grain or subgrain boundaries, visible microcracks, altered or retrogressed regions were sampled.

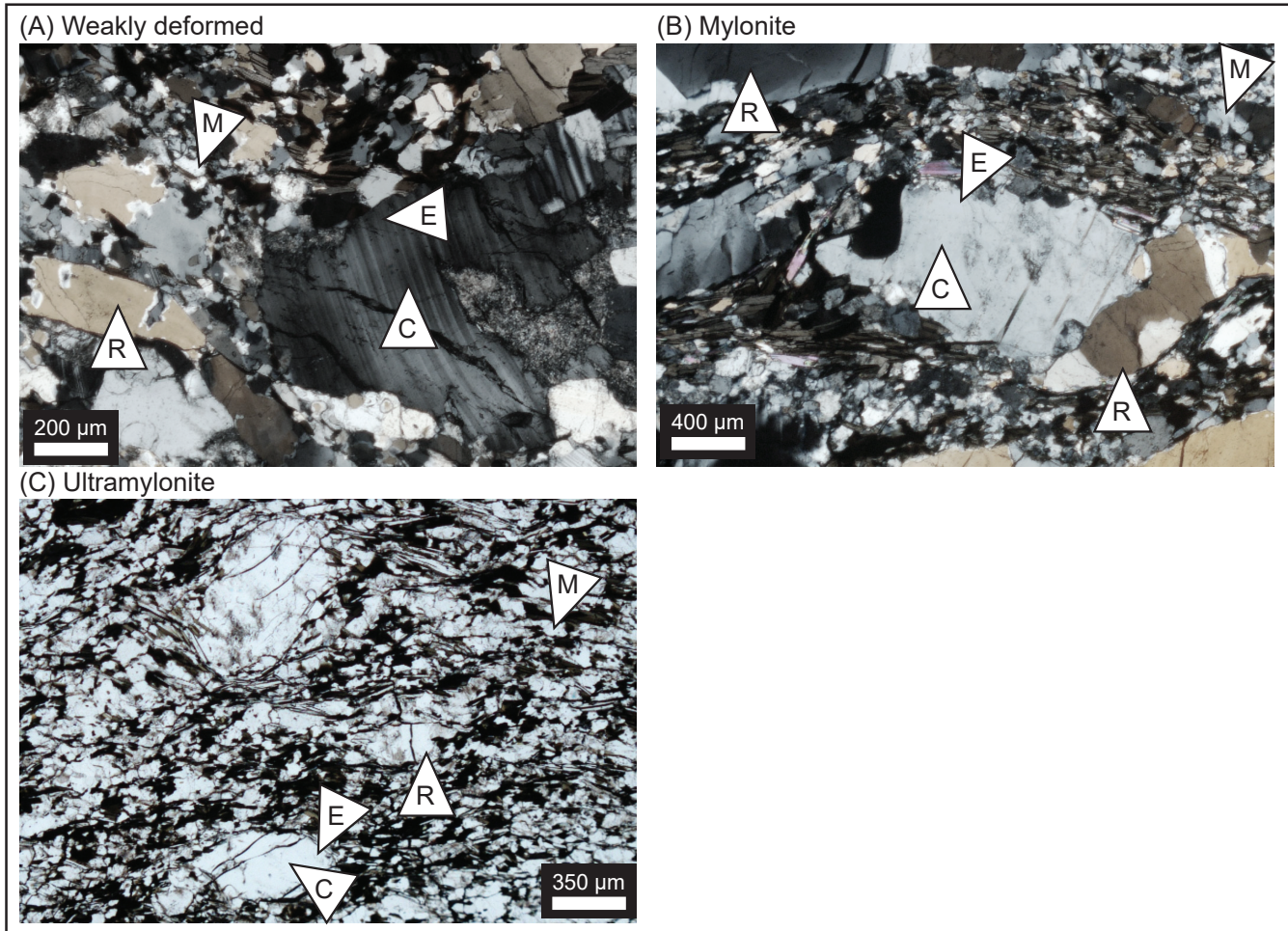


**Fig. DR2.** Representative photomicrographs of (A) weakly-deformed (SQ183a; cross-polarised light), (B) mylonitic (SQ32a, cross-polarised light), and (C) ultramylonitic (SQ32b; plane-polarised light) samples. Arrows indicate example location of analysed spots in ribbons (R), porphyroclast cores (C), porphyroclast edges (E), and the matrix (M).

TABLE DR2. SAMPLE DATA AND RESULTS FOR FELDSPAR GRAINS

Deformation Intensity	Position	Sample	Thickness (cm)	n	Mean (H:10 <sup>6</sup> Si, Al)	Standard deviation
Weakly-deformed rocks	Matrix	sq183a	0.0051	32	1993	1293
		sq183b	0.0050	6	3093	701
		Overall		36	2233	1268
	Porphyroclast edge	sq183a	0.0051	4	2460	493
		sq183b	0.0050	11	2561	608
		sq77a	0.0057	10	4554	3203
		Overall		25	3342	2248
	Porphyroclast core	sq183a	0.0051	9	1654	611
		sq183b	0.0050	4	2990	442
		sq77a	0.0057	2	1620	32
		Overall		15	2006	796
	Matrix	sq30a	0.0051	12	1783	573
sq32a		0.0055	25	1332	487	
sq187d		0.0049	32	1417	668	
Overall			66	1455	609	
Mylonites	Porphyroclast edge	sq30a	0.0051	9	1399	1315
		sq32a	0.0055	8	1428	373
		sq187d	0.0049	2	1977	1561
		Overall		19	1472	995
Porphyroclast core	sq30a	0.0051	9	1336	708	
	sq32a	0.0055	5	1767	686	
	sq187d	0.0049	11	2028	1002	
	Overall		25	1727	874	
Matrix	sq29b	0.0076	25	967	416	
	sq32b	0.0069	27	1136	574	
	sq32c	0.0067	7	995	333	
	sq79a	0.0069	11	1152	430	
	sq83	0.0052	22	1601	657	
	Overall		92	1193	571	
Ultramylonites	Porphyroclast edge	sq29b	0.0076	6	306	235
		sq32b	0.0069	13	1143	352
		sq32c	0.0067	12	645	205
		sq79a	0.0069	8	543	128
		sq83	0.0052	4	773	315
		Overall		43	741	387
Porphyroclast core	sq29b	0.0076	6	722	721	
	sq32b	0.0069	12	1071	372	
	sq32c	0.0067	8	488	146	
	sq79a	0.0069	9	629	170	
	sq83	0.0052	11	1205	689	
	Overall		46	870	533	

The sample was placed on the microscope stage and the aperture adjusted to 50  $\mu\text{m}$  square. Although a plastic guard was lowered to reduce atmospheric influence, sharp spikes in the absorption spectra indicate the presence of a small amount of atmospheric  $\text{H}_2\text{O}$  but this does not affect measurement of the broadband absorption for liquid water (Post and Tullis, 1998). Once the microscope was focussed and aligned the sample was moved out of the beam path and a background spectrum was taken. The concentration of OH and  $\text{H}_2\text{O}$  in quartz was calculated as the integral area under the broad peak between 2800 to 3800  $\text{cm}^{-1}$  using the integral absorbance version of the Beer-Lambert law:

$$A = k \cdot C \cdot t. (1)$$

Where  $A$  is the integrated absorbance ( $\text{cm}^{-1}$ ),  $k$  is the integral molar absorption coefficient of the molecule absorbing the radiation ( $\text{mol}^{-1} \text{cm}^{-2}$ ),  $C$  is the water concentration in the sample (H:10<sup>6</sup> Si), and  $t$  is the thickness of the sample. The calibration factor,  $k$ , and the calibration method were as per Gleason and DeSisto (2008) and Kronenberg and Wolf (1990).

To calculate water concentration in feldspar a modified version of the Beer-Lambert law in (1) was used as follows:

$$A = k \cdot c \cdot t. (2)$$

Where  $c$  is the water content in ppm

$\text{H}_2\text{O}$  to  $\text{KAlSi}_3\text{O}_8$  by weight and the value of  $k$  is  $15.3 \pm 0.7 \text{ ppm}^{-1} \text{ cm}^{-2}$  (Johnson and Rossman, 2003). Water concentration in ppm was multiplied by 7.72 to obtain concentrations in H:10<sup>6</sup> Si, Al. Example spectra from a quartz grain and a feldspar grain are shown in Fig. DR3.

## SUPPLEMENTARY RESULTS

### CPO of quartz

Protomylonites and mylonites reveal a shift from moderate single girdle maxima oriented normal to the X-axis, to a dominant single maximum parallel to the Y-axis (Fig. DR4). This suggests a transition from combined crystal slip along  $\{r\}\langle a \rangle$  (rhomb- $\langle a \rangle$ ) and  $\{m\}\langle a \rangle$  (prism- $\langle a \rangle$ ) in protomylonite, towards dominant prism- $\langle a \rangle$  slip in mylonite (Schmid and Casey, 1986). Ultramylonites, by contrast, comprise weaker  $c$ -axis distributions, from which no discernible slip system maxima can be identified.

Overall, our results demonstrate a systematic weakening of the  $c$ -axis distribution towards ultramylonite, concomitant with grain size reduction (Finch et al. 2015) and homogenisation of the matrix (Fig. DR1). Combined, these microstructural changes suggest a rheological switch from grain-size insensitive creep (e.g. dislocation glide and climb) to grain-size sensitive creep mechanisms (e.g. diffusion creep and grain boundary sliding). This rheological switch is a common observation in polymineralic ultramylonite rocks (Flier-voet et al., 1997; Kilian et al., 2011; Linckens et al., 2011). Dissolution-precipitation may also contribute to

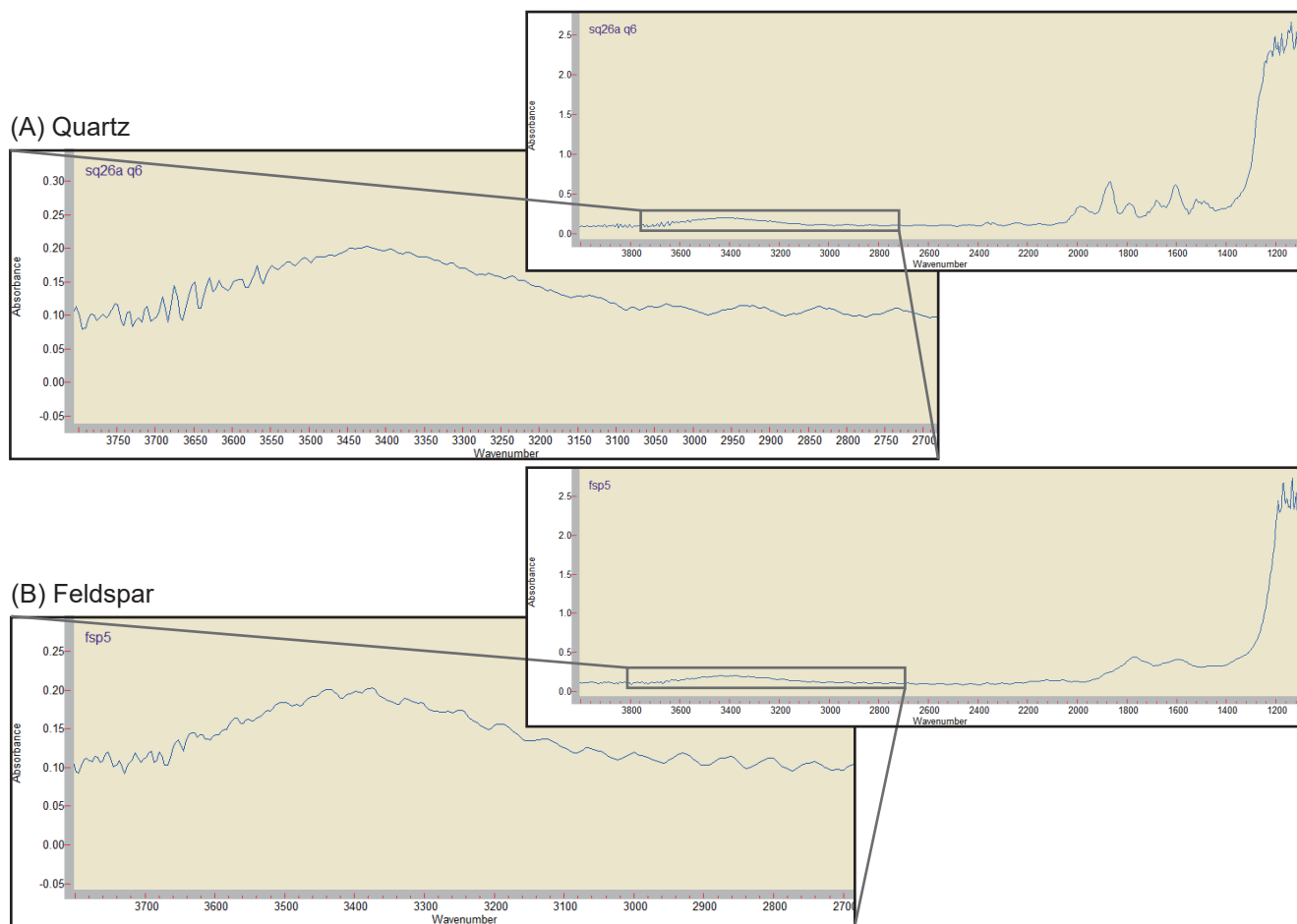


**Fig. DR3.** Example spectra from (A) a quartz grain, and (B) a feldspar grain. Insets show zoom-in of the broad peak between 2800 and 3800  $\text{cm}^{-1}$ .

homogenisation of the matrix, similar to Kilian et al. (2011), but we do not see strong evidence for it.

As outlined in the manuscript, concomitant with the change in CPO and progressive homogenisation of the matrix, there is a decrease in the grain size. The matrix of protomylonitic and mylonitic rocks has a mean quartz grain size of  $95 \pm 20 \mu\text{m}$  and mica grain size of  $170 \pm 60 \mu\text{m}$ , whereas ultramylonites show a mean quartz grain size of  $60 \pm 10 \mu\text{m}$  and mean mica grain size of  $120 \pm 40 \mu\text{m}$  (Finch et al., 2015). Quartz ribbons decrease in length from  $\sim 1.75 \text{ mm}$  in protomylonites, to  $1.5 \text{ mm}$  in mylonites, and  $<0.5 \text{ mm}$  in ultramylonites. The minimum diameter of porphyroclasts also decreases from  $3.8 \pm 2.5 \text{ mm}$  in weakly deformed orthogneisses and protomylonites, to  $3.3 \pm 2 \text{ mm}$  in mylonites, to  $1.85 \pm 1.3 \text{ mm}$  in ultramylonites.

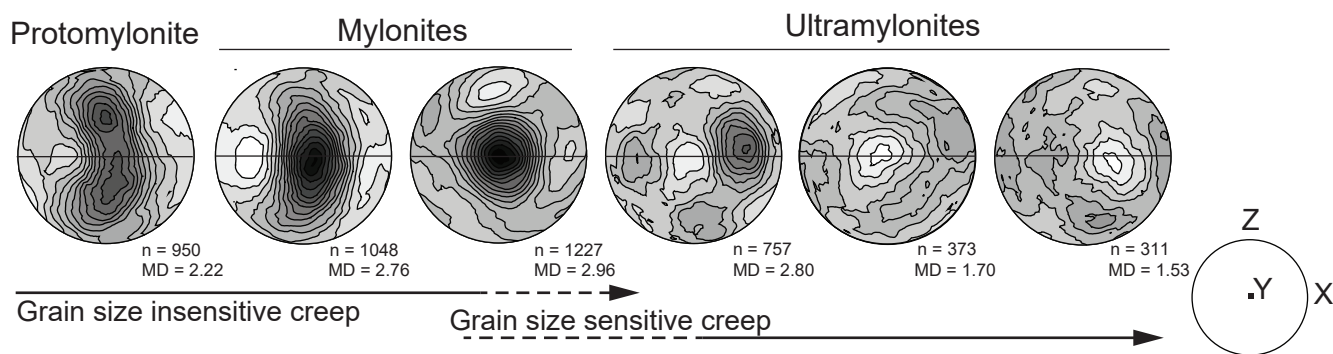


**Fig. DR4.** Variations in the quartz  $c$ -(0001) axis distribution from protomylonite to ultramylonite. Data is contoured at an interval of 0.16 times the uniform distribution. Number of grains is denoted by  $n$ . Maximum density (MD) denotes the highest multiple of uniform distribution. Pole figures are normalised to the sample with the highest MD (third sample from left). Inset shows the geometric coordinates for the pole figures (see text). Note the systematic weakening of the distribution towards ultramylonite.

## Water content in quartz and feldspar

To test the differences in molar water concentration between three levels of the independent variable (mylonitisation intensity) a one-way analysis of variance (ANOVA) would typically be employed. However, the standard version of ANOVA assumes that data are normally distributed and homoscedastic and preliminary tests indicated that these assumptions were violated. Consequently Welch's one-way ANOVA (Welch, 1951) was employed as it is robust to violations of these assumptions and widely considered to be the best alternative (e.g. Grissom, 2000; Lix et al., 1996). This test determines whether there is a difference between any of the three groups in mylonitisation intensity (main effect of the independent variable), but does not determine the locus of the effect (i.e., which groups are statistically different from each other). ANOVAs determine the ratio between the variance between groups and variance within groups (the F statistic), which is close to 1 if groups are not statistically different from one another. The test weights the variance by the degrees of freedom (number of observations in each group minus 1) and, based on the value of the F-statistic, determines the likelihood that the differences between groups occurred by chance ( $p$  value), with values less than 5% ( $p < 0.05$ ) usually taken to indicate statistical significance. If a significant main effect is determined, post-hoc tests are then employed to determine which of the three groups are significantly different from each other. A post-hoc test compares the mean and variance in each group to every other group to investigate which groups are statistically different from each other. This procedure reduces the type-1 error rate, which is the chance of falsely rejecting the null hypothesis, that is, the chance of obtaining a significant result when there is no significant difference. The type-1 error rate is reduced because the likelihood of falsely rejecting the null hypothesis is 5% with every test performed. Performing one omnibus test initially (ANOVA) means there is only a 5% chance of a type-1 error. If a significant result is obtained, multiple tests between groups (post-hoc tests) are then performed and although the type-1 error rate is then elevated (to ~14.3% for three tests), it is already known with 95% certainty (from the ANOVA) that at least two groups must be significantly different, thus reducing the risk. The test used in this study, the Games-Howell test (Games and Howell, 1976), is similar to other post-hoc tests but it takes the sample size and variance of each group into account when calculating the error and degrees of freedom. Consequently, this test is used when the variance in each group and the group size are unequal and only requires that there are  $>6$  observations in each group.

Separate analyses were performed for quartz in the matrix and in ribbons (Fig. DR5A). Analysis indicates that there is a significant main effect of mylonitisation intensity for matrix quartz ( $F = 15.636$  (degrees of freedom between groups= 2, within groups= 50.102),  $p < 0.05$ ) and for quartz ribbons ( $F (2, 48.393) =$

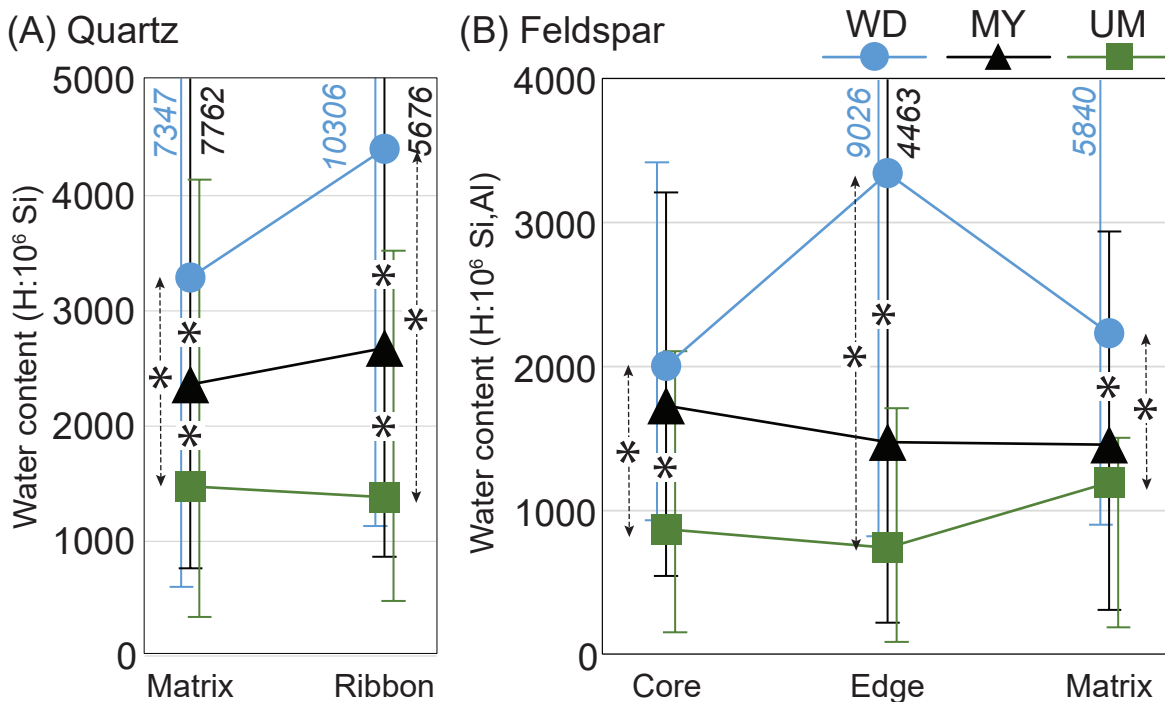
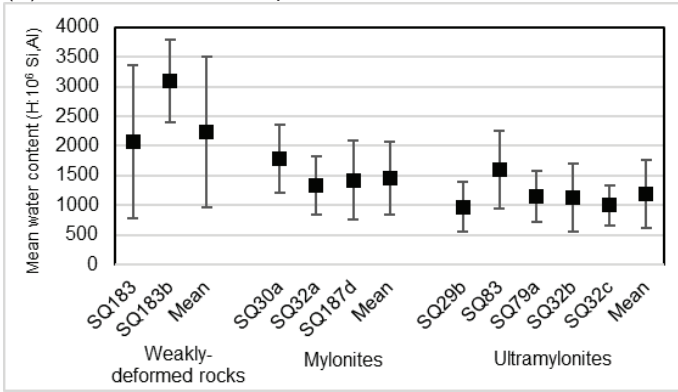
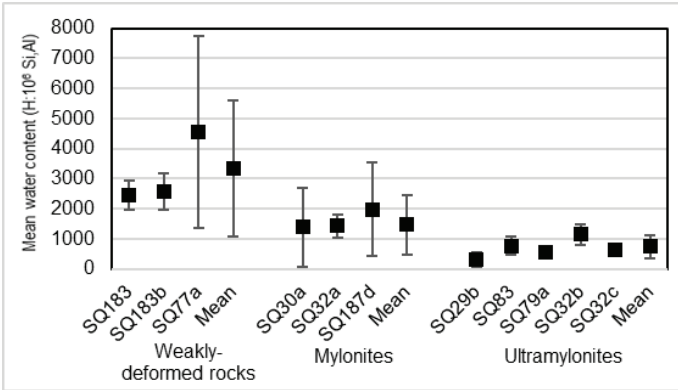


**Fig. DR5.** Mean water content in A: quartz (matrix and ribbons) and B: feldspar (porphyroclast cores, porphyroclast edges, and matrix) for weakly-deformed rocks (WD), mylonites (MY), and ultramylonites (UM). Error bars are the minimum and maximum values and the uppermost value is listed above the graph when beyond the maximum y-value. Stars indicate statistically significant differences between means ( $p < 0.05$ ).

(A) Water content in feldspar in the matrix



(B) Water content in the edges of feldspar porphyroclasts



(C) Water content in the cores of feldspar porphyroclasts

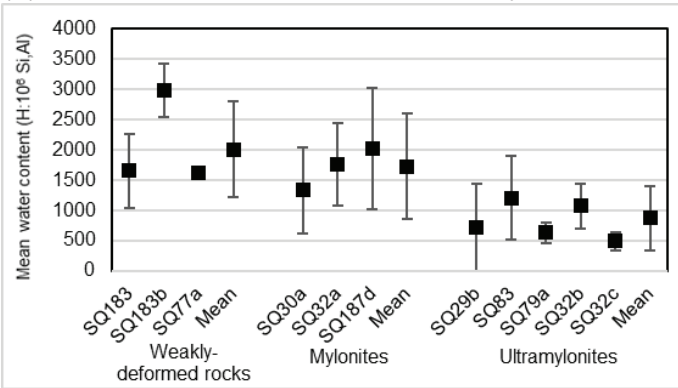


**Fig. DR6.** Graphs of mean water content for each sample in each rock group for (A) feldspar in the matrix, (B) porphyroclast edges, and (C) porphyroclast cores. Error bars are one standard deviation from the mean. Figures show a decrease in both the average water content and the uncertainty as strain increases to the right.

water content in porphyroclast cores showed a different pattern: while ultramylonites (mean = 870 H:10<sup>6</sup> Si) contained significantly less water than weakly deformed rocks (mean = 2006 H:10<sup>6</sup> Si), there was no significant difference between weakly deformed rocks and mylonites (mean = 1727 H:10<sup>6</sup> Si). There was also a significant difference between mylonites and ultramylonites.

In order to investigate whether water content is related to porphyroclast size we determined the degree of linear correlation between the minimum diameter of porphyroclasts and their water content using

the Pearson product-moment correlation coefficient (Pearson, 1895). This analysis determines a value (*R*) between +1 and -1 inclusive where 0 is no correlation, 1 is total positive correlation, and -1 is total negative correlation. The results in Table DR3 indicate no or low correlation for all relationships except between the water content in porphyroclast cores and porphyroclast size in mylonites and ultramylonites.

TABLE DR3. PEARSON'S CORRELATION COEFFICIENTS

	Porphyroclast edge*	Porphyroclast core†
Weakly-deformed rocks	0.0200	0.0888
Mylonites	0.1456	0.3343
Ultramylonites	-0.0425	0.4423

Notes:

\*Porphyroclast edge water content vs. porphyroclast size

†Porphyroclast core water content vs. porphyroclast size

36.865,  $p < 0.05$ ). Post-hoc comparisons using the Games-Howell test indicated that matrix quartz in ultramylonites (mean = 1455 H:10<sup>6</sup> Si) contained significantly less water than quartz in weakly-deformed rocks (mean = 3264 H:10<sup>6</sup> Si) and mylonites (mean = 2336 H:10<sup>6</sup> Si; Figs. 2, DR5). The difference between mylonites and weakly deformed rocks was not significant. Similarly, there was significantly less water in quartz ribbons in ultramylonites (mean = 1357 H:10<sup>6</sup> Si) than weakly-deformed rocks (mean = 4387 H:10<sup>6</sup> Si) and mylonites (mean = 2657 H:10<sup>6</sup> Si; Figs. 2, DR5). The difference between the water content in quartz ribbons in weakly deformed rocks and mylonites was also significant.

Analyses in feldspar were separated into matrix feldspar, porphyroclast edges, and porphyroclast cores (Figs. DR5B, DR6). Analysis indicates that there is a significant main effect of mylonitisation intensity for matrix feldspar ( $F(2, 86.473) = 12.055, p < 0.05$ ), for porphyroclast edges ( $F(2, 29.829) = 20.244, p < 0.05$ ), and for porphyroclast cores ( $F(2, 30.184) = 19.949, p < 0.05$ ). Post-hoc comparisons using the Games-Howell test indicated that matrix feldspar in ultramylonites (mean = 1193 H:10<sup>6</sup> Si) contained significantly less water than matrix feldspar in weakly-deformed rocks (mean = 2440 H:10<sup>6</sup> Si; Figs. 2, DR6). There was also a significant difference between water content in matrix feldspar in weakly deformed rocks and mylonites (mean = 1455 H:10<sup>6</sup> Si; Figs. 2, DR6). The difference between mylonites and ultramylonites was not significant. Similarly, post-hoc comparisons for the water content on porphyroclast edges indicates that ultramylonites (mean = 741 H:10<sup>6</sup> Si) contained significantly less water than weakly-deformed rocks (mean = 3342 H:10<sup>6</sup> Si; Figs. 2, DR6) but the difference between ultramylonites and mylonites (mean = 1472 H:10<sup>6</sup> Si) was not significant. There was also a significant difference between weakly deformed rocks and mylonites. Post-hoc tests on the

## References

- Finch, M. A., Weinberg, R. F., Fuentes, M. G., Hasalova, P., and Becchio, R., 2015, One kilometre-thick ultramylonite, Sierra de Quilmes, Sierras Pampeanas, NW Argentina: *Journal of Structural Geology*, v. 72, p. 33-54.
- Fliervoet, T. F., White, S. H., and Drury, M. R., 1997, Evidence for dominant grain-boundary sliding deformation in greenschist- And amphibolite-grade polyminerale ultramylonites from the Redbank Deformed Zone, Central Australia: *Journal of Structural Geology*, v. 19, no. 12, p. 1495-1520.
- Games, P. A., and Howell, J. F., 1976, Pairwise Multiple Comparison Procedures with Unequal N's and/or Variances: A Monte Carlo Study: *Journal of Educational Statistics*, v. 1, no. 2, p. 113-125.
- Gleason, G. C., and DeSisto, S., 2008, A natural example of crystal-plastic deformation enhancing the incorporation of water into quartz: *Tectonophysics*, v. 446, no. 16-30.
- Grissom, R. J., 2000, Heterogeneity of Variance in Clinical Data: *Journal of Consulting & Clinical Psychology*, v. 68, no. 1, p. 155-165.
- Johnson, E. A., and Rossman, G. R., 2003, The concentration and speciation of hydrogen in feldspars using FTIR and <sup>1</sup>H MAS NMR spectroscopy: *American Mineralogist*, v. 88, p. 901-911.
- Kilian, R., Heilbronner, R., and Stunitz, H., 2011, Quartz grain size reduction in a granitoid rock and the transition from dislocation to diffusion creep: *Journal of Structural Geology*, v. 33, no. 8, p. 1265-1284.
- Kronenberg, A. K., and Wolf, G. H., 1990, Fourier transform infrared spectroscopy determinations of intragranular water content in quartz-bearing rocks: implications for hydrolytic weakening in the laboratory and within the earth: *Tectonophysics*, v. 172, no. 3-4, p. 255-271.
- Linckens, J., Herwegh, M., Müntener, O., and Mercolli, I., 2011, Evolution of a polyminerale mantle shear zone and the role of second phases in the localization of deformation: *Journal of Geophysical Research: Solid Earth*, v. 116, no. B6, p. B06210.
- Lix, L. M., Keselman, J. C., and Keselman, H. J., 1996, Consequences of assumption violations revisited: A quantitative review of alternatives to the one-way analysis of variance F test: *Review of Educational Research*, v. 66, no. 4, p. 579-619.
- Pearson, K., 1895, Contributions to the mathematical theory of evolution. Note on reproductive selection: *Proceedings of the Royal Society of London*, v. 59, p. 300-305.
- Post, A. D., and Tullis, J., 1998, The rate of water penetration in experimentally deformed quartzite: implications for hydrolytic weakening: *Tectonophysics*, v. 295, p. 117-137.
- Schmid, S. M., and Casey, M., 1986, Complete fabric analysis of some commonly observed quartz C-axis patterns, *Mineral and Rock Deformation: Laboratory Studies, Volume 36*: Washington, DC, AGU, p. 263-286.
- Welch, B. L., 1951, On the comparison of several mean values: An alternative approach: *Biometrika*, v. 38, p. 330-336.
- Wilson, C. J. L., Russell-Head, D. S., Kunze, K., and Viola, G., 2007, The analysis of quartz c-axis fabrics using a modified optical microscope: *Journal of Microscopy*, v. 227, no. 1, p. 30-41.